Journal of CO2 Utilization 80 (2024) 102702

Contents lists available at ScienceDirect

Journal of CO2 Utilization

journal homepage: www.elsevier.com/locate/jcou

Mesoporous phenolic/carbon materials templated by CO_2-based PEO-*b*-PCHC diblock copolymers through mediated competitive intermolecular hydrogen bonding interactions for CO_2 capture

Wei-Ting Du, Shih-Yun Chen, Shiao-Wei Kuo *

Department of Materials and Optoelectronic Science, Center for Functional Polymers and Supramolecular Materials, National Sun Yat-Sen University, Kaohsiung 80424, Taiwan

ARTICLE INFO

Keywords:
CO_2-based block copolymer
Hydrogen bonding
Self-assembled structure
Mesoporous material
CO_2 capture

ABSTRACT

The CO_2-based diblock copolymer, poly(ethylene oxide-*b*-cyclohexene carbonate) (PEO-*b*-PCHC), was synthesized via ring opening copolymerization (ROCOP) by using PEO as a macro-chain-transfer agent. Theses diblock copolymers were comprehensive characterized by Fourier-transform infrared (FTIR) and nuclear magnetic resonance (NMR) spectroscopy, differential scanning calorimetry (DSC) and thermogravimetric analysis (TGA) to gain insights into their chemical structures and thermal properties. The microphase separation was induced after blending with phenolic resin through medicated by competitive hydrogen bonding interaction between phenolic hydroxyl (OH) group with ether unit of PEO and C═O unit of PCHC based on FTIR analyses. Small angle X-ray scattering (SAXS) analyses also provided the self-assembled structures of specific phenolic/PEO-*b*-PCHC blends following thermal polymerization at 180 °C because of the reaction-induced microphase separation mechanism. Upon removal of PEO-*b*-PCHC diblock copolymer templates at 350 °C, mesoporous phenolic resins including cylindrical, spherical and worm-like structures were obtained based on SAXS, transmission electron microscope (TEM) and nitrogen adsorption/desorption analyses. Furthermore, the mesoporous carbons were further obtained from mesoporous phenolic resin thermal calcined at 700 °C under N_2 atmosphere. These carbonized mesoporous materials exhibited impressive characteristics such as high surface areas and they demonstrated effective CO_2 capture capabilities (4.5 mmol g^{-1} at 273 K). The captured CO_2 could subsequently be employed in ROCOP again for synthesizing CO_2-based copolymers, aligning with the principles of a circular economy.

1. Introduction

There has been extensively investigated into the self-assembled structures by diblock copolymers over the past last three decades due to their possible applications in photonic crystals [1,2], drug deliveries [3], nanocomposites [4], and nanopatterns [5]. In addition, one common approach is to utilize block copolymers as templates to synthesize mesoporous phenolic or silica materials with pore size ranging from 2 to 50 nm, particularly using poly(ethylene oxide)-based block copolymers such as P123 [6], F127 [7,8], PEO-*b*-PCL [9–14], PEO-*b*-PMMA [15], PEO-*b*-PLA [16,17], PEO-*b*-PS[18–20], PEO-*b*-P4VP [21], and PEO-*b*-PBLG [22]. For instance, in our previous decade-long studies, we have successfully used PEO-*b*-PCL as templates to provide highly ordered mesoporous phenolic/carbon materials through the combination of thermal polymerization and carbonization process with well-defined cylindrical, spherical, and double gyroid structures [23–28].

In light of the substantially environmental damage due to the human activities, there is a growing interest in biodegradable plastics as an alternative approach to traditional petrochemical plastics. However, poly(lactide acid) (PLA) or poly(caprolactone) (PCL) has been commercially available, it still cannot completely replace traditional petrochemical plastics. There is another emerging opportunity to synthesize polycarbonates from epoxide and carbon dioxide (CO_2), aiming to achieve the balance between human life and environmental sustainability. What makes this way even more intriguing is the use of a new PEO-based diblock copolymer derived from CO_2 as the template to prepare mesoporous phenolic/carbon materials, to the best of our knowledge, has not been previously proposed. The main challenge is used CO_2 for this purpose is difficult to react with other molecules. To address this issue, the ring opening copolymerization (ROCOP) becomes

* Corresponding author.
E-mail address: kuosw@faculty.nsysu.edu.tw (S.-W. Kuo).

https://doi.org/10.1016/j.jcou.2024.102702
Received 16 November 2023; Received in revised form 25 January 2024; Accepted 4 February 2024
Available online 8 February 2024

the crucial technique to reduce the activation energy required for CO_2 to take part in the chemical reaction. This concept draws inspiration from PLA and PCL by using successful ring opening polymerization (ROP) [29–32]. The design of catalyst for both ROP and ROCOP is highly similar, both employing a coordination-insertion polymerization mechanism [33–35]. Therefore, researchers with expertise in ROP was transferred their skills and knowledge to the field of CO_2 copolymerization [36–41]. In addition to studying catalysts for ROCOP, it is also crucial to explore the various applications of these polycarbonates made from CO_2 in various fields to reduce environmental impact.

Various block copolymers synthesized through ROCOP have been explored; for example, Darensbourg and co-workers demonstrated that the addition of excess H_2O could lead to the reduction in the molecular weight for poly(propylene carbonate) (PPC) and confirm the presence of hydroxyl (OH) group at the chain end. Then 1,8-diazabicylco[5.4.0] undec-7-ene (DBU) and lactide monomers were added to synthesize PLA-*b*-PPC-*b*-PLA triblock copolymers [42]. Williams et al. found a new route to create copoly(ester-*b*-carbonate-*b*-ester). The dinuclear zinc catalyst can be used to obtained PCHC and PCL, respectively. Thus, the presence of the catalyst and all three monomers (cyclohexene oxide, CL, CO_2) in the autoclave reactor could achieve triblock copolymer of PCL-*b*-PCHC-*b*-PCL in one pot dramatically [43]. In addition, a macro-CTA including PEO, poly(propylene oxide) (PPO), and polystyrene (PS) was used to prepare CO_2-based diblock copolymers by classic catalyst systems such as (BDI)ZnOAc and SalenCoTFA/PPN-TFA for this purpose [44].

In this study, PEO acts as a macro-CTA and LZn_2OAc_2 was reacted with CHO and CO_2 to form two different molecular weights of PEO-*b*-PCHC diblock copolymers as shown in Fig. 1(a), which are comprehensive characterized to confirm their chemical structures by FTIR, ^1H and ^{13}C NMR spectroscopy. As the templates, these diblock copolymers are blended with resol-type phenolic resin with various compositions to form phenolic/PEO-*b*-PCHC blends. In our previously studies [9,21, 45–49], we have widely discussed about all the possibility of A-*b*-B/C blends through mediated hydrogen bonding interactions. The key factor in achieving self-assembled structures in these blends depends strongly on the varying strength of hydrogen bonding or inter-association equilibrium constant (K_A) between A/B, A/C and B/C binary pairs [9]. For example, the use of PEO-*b*-PCL diblock copolymer as template to prepare the mesoporous phenolic material is strongly dependent on the phenolic or phenolic derivative compositions because of the different K_A values for PEO (K_A = 280) and PCL (K_A = 116) [50]. In addition, the PLA_{440}-*b*-PEO_{454}-*b*-PLA_{440} triblock copolymer with high molecular weight was also synthesized as templates to provide large mesoporous phenolic/carbon (> 50 nm) and high specific surface area (> 600 $m^2 g^{-1}$), which could be used for CO_2 capture and supercapacitor applications [17]. The other templates made from block copolymers with special mesoporous structures such as dual porous structure or even Frank-Kasper phase were also summarized in our previous literatures [9,21].

In our previous study, the hydrogen bonding interaction OH units of phenolic derivative with C═O units of PCHC have been discussed and we found much weaker K_A value (K_A = 5) [51] and thus we could expect that the OH units of phenolic was preferred to interact with ether units of PEO rather than C═O units of PCHC and thus the PCHC segment would form the microphase separation and self-assembled structure from the miscible phenolic/PEO domains at relative lower phenolic compositions. In this current study, the mesoporous phenolic/carbon materials could be obtained after thermal pyrolysis of PEO-*b*-PCHC at 350 °C or carbonization at 700 °C, respectively, as confirmed by SAXS and TEM analyses. These resulting carbonized mesoporous materials could form remarkable characteristics including high surface areas and pore volumes and they demonstrated effective CO_2 capture capabilities.

2. Experimental section

2.1. Materials

Poly(ethylene glycol) methyl ether (PEO) with an average molecular weight (M_n) of 5000 was procured from Sigma Aldrich. Calcium hydride (CaH_2) was obtained from Alfa Aesar, while sodium hydroxide (NaOH), hydrochloric acid (HCl), and cyclohexene oxide (CHO) was purchased from SHOWA. Prior to use, CHO was refluxed with CaH_2. CO_2 (>99.999%) was ordered from Hsin E Li Gas Industrial Co., Ltd. Tetrahydrofuran (THF), methanol (MeOH), dichloromethane (DCM), *n*-hexane were sourced from Thermo Fisher Scientific. The catalyst $LZn_2(OAc)_2$ was confirmed from our previous literature [51].

2.2. Copolymerization of CO_2 and CHO based on PEO as a macro-chain-transfer agent

PEO (1.0 g) and $LZn_2(OAc)_2$ (0.046 g or 0.023 g) as the initiator and catalyst, respectively, were added into the autoclave equipped with the stirring bar and connected with the vacuum line. This reaction was dried at 50 °C for 10 h under the vacuum. The autoclave was purged with CO_2

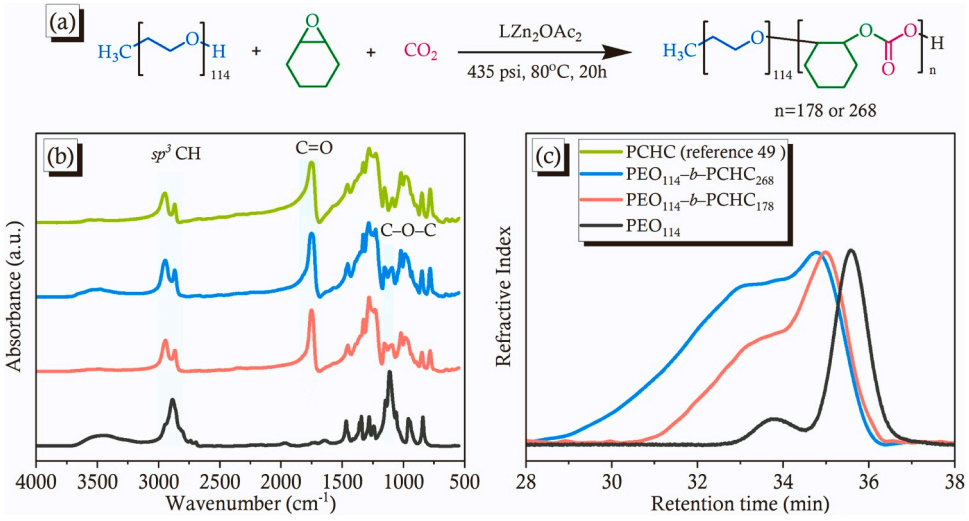

Fig. 1. (a) The synthesis of PEO-*b*-PCHC diblock copolymers, and their corresponding (b) FTIR, (c) GPC analyses of PEO_{114}-*b*-$PCHC_{268}$, PEO_{114}-*b*-$PCHC_{178}$ diblock copolymers, and pure PEO_{114}.

gas and CHO (7.1 mL) was then injected. The ROCOP was carried out at a constant CO_2 pressure of 435 psi at 80 °C for 20 h. The reactor was then cooled, and the excess CO_2 was carefully released. This crude was dissolved in DCM and extracted with 5% HCl aqueous solution. Finally, the solution was precipitated several times in hexane. The PEO_{114}-*b*-$PCHC_{178}$ and PEO_{114}-*b*-$PCHC_{268}$ diblock copolymers were obtained and then dried in a vacuum oven as the white powder. ^{1}H NMR (500 MHz, $CDCl_3$, δ, ppm): 4.65 (CyC**H**), 3.63 (C**H**$_2$O), 1.16–2.27 (CyC**H**$_2$) for PEO_{114}-*b*-$PCHC_{268}$. 4.66 (CyC**H**), 3.63 (C**H**$_2$O), 1.16–2.27 (CyC**H**$_2$) for PEO_{114}-*b*-$PCHC_{178}$; ^{13}C NMR (125 MHz, $CDCl_3$, δ, ppm): 154.57 (C═O), 76.85 (Cy**C**H), 70.85 (**C**H$_2$O), 20.77–31.39 (Cy**C**H$_2$). for PEO_{114}-*b*-$PCHC_{268}$. 154.58 (C═O), 76.86 (Cy**C**H), 70.87 (**C**H$_2$O), 20.77–31.39 (Cy**C**H$_2$) for PEO_{114}-*b*-$PCHC_{178}$; FTIR (KBr, cm^{-1}): 1751 (C═O) for PEO_{114}-*b*-$PCHC_{268}$ and PEO_{114}-*b*-$PCHC_{178}$; GPC: M_n = 31000 g mol^{-1}, PDI = 1.43 for PEO_{114}-*b*-$PCHC_{268}$. M_n = 26000 g mol^{-1}, PDI = 1.23 for PEO_{114}-*b*-$PCHC_{178}$.

2.3. Self-assembled phenolic/PEO-b-PCHC blends and mesoporous phenolic/carbons

The resol-type phenolic resin, which was reported by our previous literature [27], was blended with various amounts of PEO-*b*-PCHC in THF. The mixtures were placed on aluminum pans and THF were slowly evaporated at room temperature for 3 days, then they were dried at 40 °C under vacuum for 1 day. The resulting samples were cured at a slow heating rate of 1 °C/min^{-1} to 150 °C and kept for 24 h. The cured samples were subsequently pyrolyzed at same heating rate to 350 °C and kept for 24 h to remove PEO-*b*-PCHC templates and then provided mesoporous phenolic resin. Mesoporous carbons were obtained through carbonization at heating rate of 1.6 °C min^{-1} to 700 °C for 2 h under nitrogen atmosphere.

3. Results and discussion

3.1. Syntheses of PEO-b-PCHC Diblock Copolymers

Diblock copolymers, namely PEO_{114}-*b*-$PCHC_{178}$ and PEO_{114}-*b*-$PCHC_{268}$, were prepared via ROCOP using $LZn_2(OAc)_2$ as the catalyst with different amounts, with the CHO group being activated to react with CO_2, employing PEO as the initiating group as shown in Fig. 1(a). The chemical structure of these diblock copolymers was characterized by FTIR, ^{1}H and ^{13}C NMR spectroscopy. Fig. 1(b) displays C═O stretching with strong absorption at 1751 cm^{-1} for PEO-*b*-PCHC diblock copolymers, indicating that linear carbonate copolymers were synthesized successfully instead of cyclic cyclohexene carbonate. The degree of polymerization (DP) of the PCHC segment could be determined by comparing the integrated area of CH_2 signal in PEO (with a number-average molecular weights, M_n = 5000) at 3.63 ppm to CH signal in PCHC at 4.65–4.66 ppm from ^{1}H NMR as displayed in Fig. S1(b). Consequently, the M_n values for PEO_{114}-*b*-$PCHC_{178}$ and PEO_{114}-*b*-$PCHC_{268}$ are approximately 30300 and 43000, respectively. Furthermore, DOSY ^{1}H NMR displays single diffusion coefficient for each polymer as Fig. S2, indicating the resulting diblock copolymers were formed successfully. The ^{13}C NMR presents the C-H signal of the cyclohexane unit within the main chain appears at 76.85–76.86 ppm, while the CH_2 signal of PEO registers at 70.85–70.87 ppm as shown in Fig. S1(c). Notably, the C═O signal at 154.57–154.58 ppm confirms the successful incorporation of CO_2 into the copolymer main chain. The graphical representation of GPC revealed a bimodal distribution for the commercial PEO as shown in Fig. 1(c). Additionally, the increase in the molecular weight of the PEO-*b*-PCHCs copolymers was observed as DP increased.

To investigate the thermal property and miscibility behavior of pure PCHC, these PEO-*b*-PCHC copolymers, and pure PEO, we employed DSC and TGA analyses. Fig. 2(a) shows a single value of T_g, which increased with the lengthening of the PCHC segment, suggesting the absence of microphase separation in the diblock copolymers. Moreover, the introduction of PCHC into the PEO segment could disrupt the polymer chain stacking, resulting in the T_m value depressed or even disappeared due to the miscibility behavior between PEO and PCHC block segment. From our

previous investigation [49], the full widths at half maximum of C═O unit in FTIR analyses of pure PCHC is 63 cm^{-1} due to intramolecular H-bonding interaction; however, PEO_{114}-*b*-$PCHC_{178}$ and

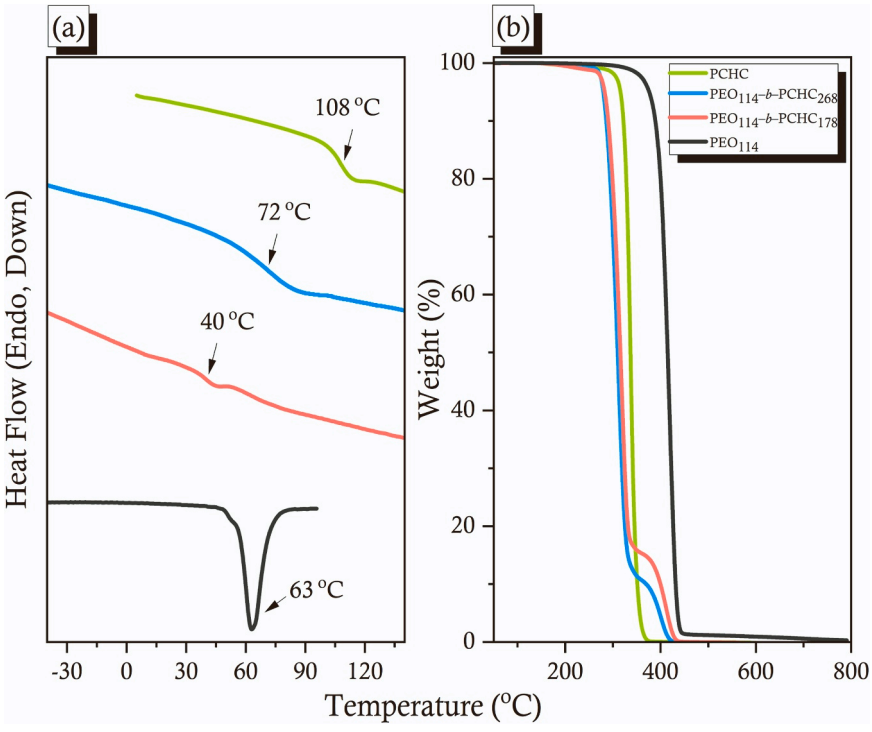

Fig. 2. (a) DSC and (b) TGA thermal analyses of PCHC, PEO_{114}-*b*-$PCHC_{268}$, PEO_{114}-*b*-$PCHC_{178}$, and PEO_{114}.

PEO_{114}-*b*-$PCHC_{268}$ exhibited 46 cm^{-1} and 56 cm^{-1}, respectively, as shown in Fig. S3(a). This indicates that the increase of weight fraction of PEO segment into the PEO-*b*-PCHC diblock copolymers, the intramolecular H-bonding interaction of pure PCHC may transfer to the weak intermolecular hydrogen bonding or dipole-dipole interaction between O-CH_2 unit from PEO segment and C═O unit from PCHC segment [52] and thus the fraction of intramolecular hydrogen bonding of C═O unit was decreased with the increase of PEO compositions as shown in Fig. S3 (b). Further evidence supporting this observation was derived from the TGA analysis presented in Fig. 2(b). Specifically, the T_{d5} value of pure PCHC (316 °C) exceeded that of PEO_{114}-*b*-$PCHC_{268}$ (280 °C) and PEO_{114}-*b*-$PCHC_{178}$ (282 °C). The difference in T_{d5} value between PEO_{114}-*b*-$PCHC_{268}$ and PEO_{114}-*b*-$PCHC_{178}$ could be attributed to the decrease in the fraction of intramolecular hydrogen bonding of C═O unit upon increasing PEO compositions and resulted in the lower thermal decomposition behavior even though the PEO segment itself possesses higher T_{d5} value (390 °C).

3.2. Thermal analyses, hydrogen bonding interaction and self-assembled structures of phenolic/PEO-b-PCHCs blends

Adjusting K_A values of two block segments within the diblock copolymers could provide a valuable development of mesoporous materials in our previous studies [48]. Specifically, we have blended phenolic resin with various diblock copolymers such as PEO-*b*-PCL (K_A = 280 for PEO, K_A = 116 for PCL) [53], PEO-*b*-PLA (K_A < 10 for PLA) [16], and PCL-*b*-P4VP (K_A = 1400 for P4VP) [54]. Fig. 3(a) presents the DSC analyses of various phenolic/PEO_{114}-*b*-$PCHC_{268}$ blends and two T_g values at relative lower phenolic compositions were observed such as phenolic/PEO_{114}-*b*-$PCHC_{268}$ = 30/70, 40/60, 50/50 and 60/40, indicating the occurrence of possible microphase separation. The initially miscible behavior of pure PEO-*b*-PCHC diblock copolymer was transformed to the immiscible behavior through the blending of phenolic resin owing to the different completive hydrogen bonding strength between phenolic/PEO (K_A = 280) and phenolic/PCHC (K_A = 5) binary pairs. As a result, the OH units of phenolic was preferred to interact with ether units of PEO rather than C═O units of PCHC and thus the PCHC segment would form the microphase separation from the miscible phenolic/PEO domains at relative lower phenolic compositions (< 60 wt%). However, further increasing phenolic compositions, the single T_g values were observed at phenolic/PEO_{114}-*b*-$PCHC_{268}$ = 80/20 and 70/30 blends, indicating good miscibility due to the OH units of phenolic were both interacted with ether units of PEO and C═O units of PCHC. The FTIR spectroscopy of the C═O units on the PCHC block segment could provide this evident as displayed in Fig. 3(b). As mentioned in our previous study [51], the positions of inter H-bonding, intra H-bonding and free C═O units of PCHC segment are located at ca. 1721, 1742 and 1761 cm^{-1}, respectively. The curve fitting results were summarized in Fig. 3(c), and the area fractions of distinct interactions were shown in Fig. 3(d). Clearly, the area percentage of intermolecular H-bonding C═O unit of PCHC

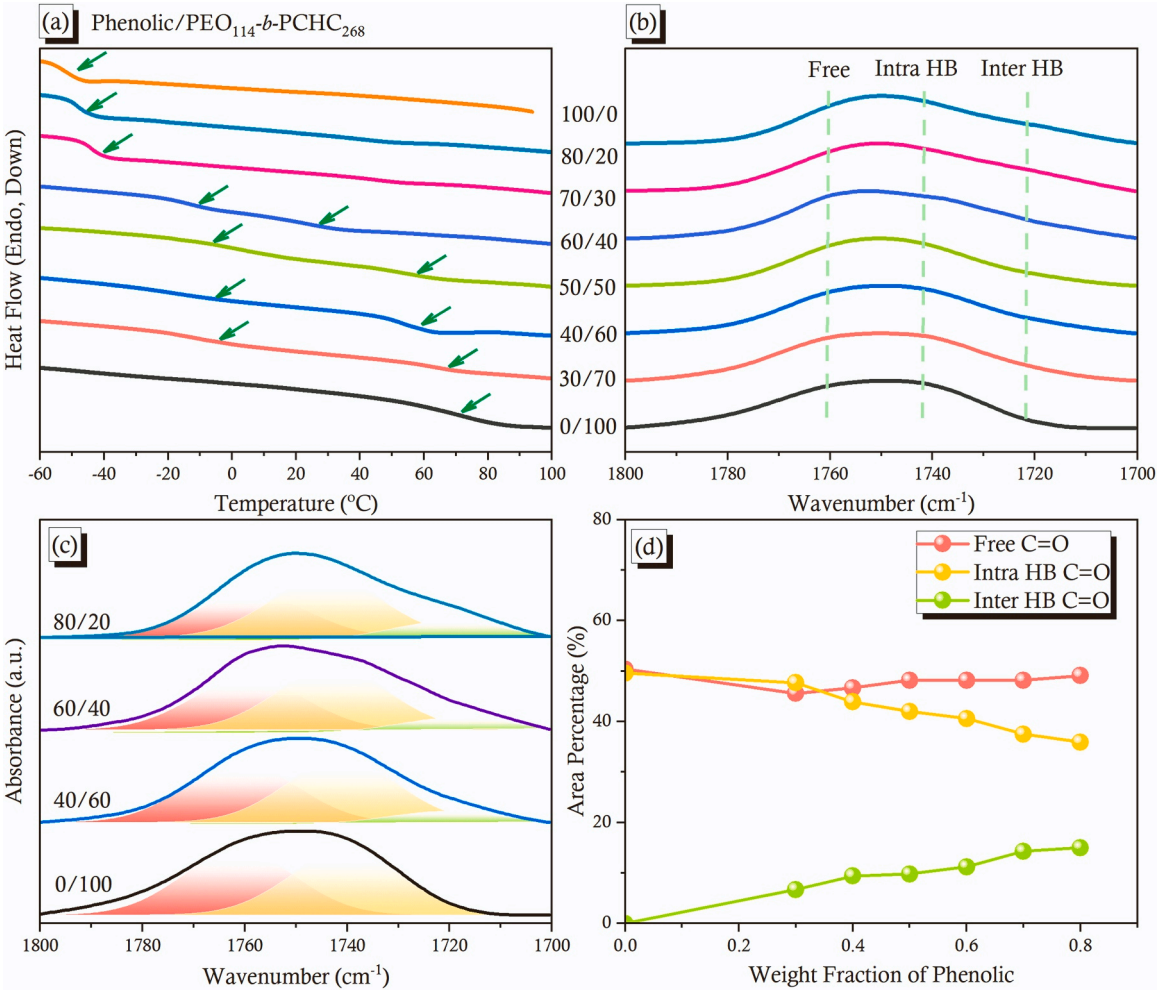

Fig. 3. (a) DSC thermal analyses and (b) the FTIR spectra of various phenolic/PEO_{114}-*b*-$PCHC_{268}$ blends, (c) The corresponding FTIR curve fitting result of various phenolic/PEO_{114}-*b*-$PCHC_{268}$ blends, and (d) The area percentage of intermolecular H-bonded C═O, intramolecular H-bonded C═O, and free C═O units of PCHC block segment.

segment was increase upon increasing phenolic concentrations and thus the phenolic/PEO_{114}-*b*-$PCHC_{268}$ = 80/20 and 70/30 blends displayed the miscible behavior at relative higher phenolic concentrations, consistent with DSC analyses.

To gain insights into the self-assembled structures at distinct ratios after blending, SAXS analyses were conducted of phenolic/PEO_{114}-*b*-$PCHC_{268}$ blends at room temperature as shown in Fig. 4(a). For pure PEO_{114}-*b*-$PCHC_{268}$, it displays the miscible disorder structure (single T_g value) without any obvious peak; however, they exhibited the clear peak ratios of $1:\sqrt{3}:\sqrt{7}$ at relative lower phenolic concentrations (<60 wt%) with cylindrical structures, which are consistent with DSC analyses with two T_g values. Furthermore, the *d*-spacing derived from the first q^* peak, as calculated using Bragg's law, exhibited an increase as the phenolic concentration rose, progressing from 29.76 nm (20 wt% phenolic) to 43.61 nm (50 wt% phenolic). The *d*-spacing was increased significantly upon increasing phenolic resin, which is attributed to form intermolecular hydrogen bonding with ether units of PEO ratio than C═O units of PCHC, which is similar with the increasing of block segment length. In addition, the compete hydrogen bonding strength between phenolic/PEO and phenolic/PCHC domain would also enhance the repulsive force between the adjacent branches of the PCHC block segment, which is believed to cause the backbone to stretch out and thus the d-spacing was increased. Further increasing the phenolic concentrations (> 60 wt%), they transform back to short-range order or a miscible disorder structure

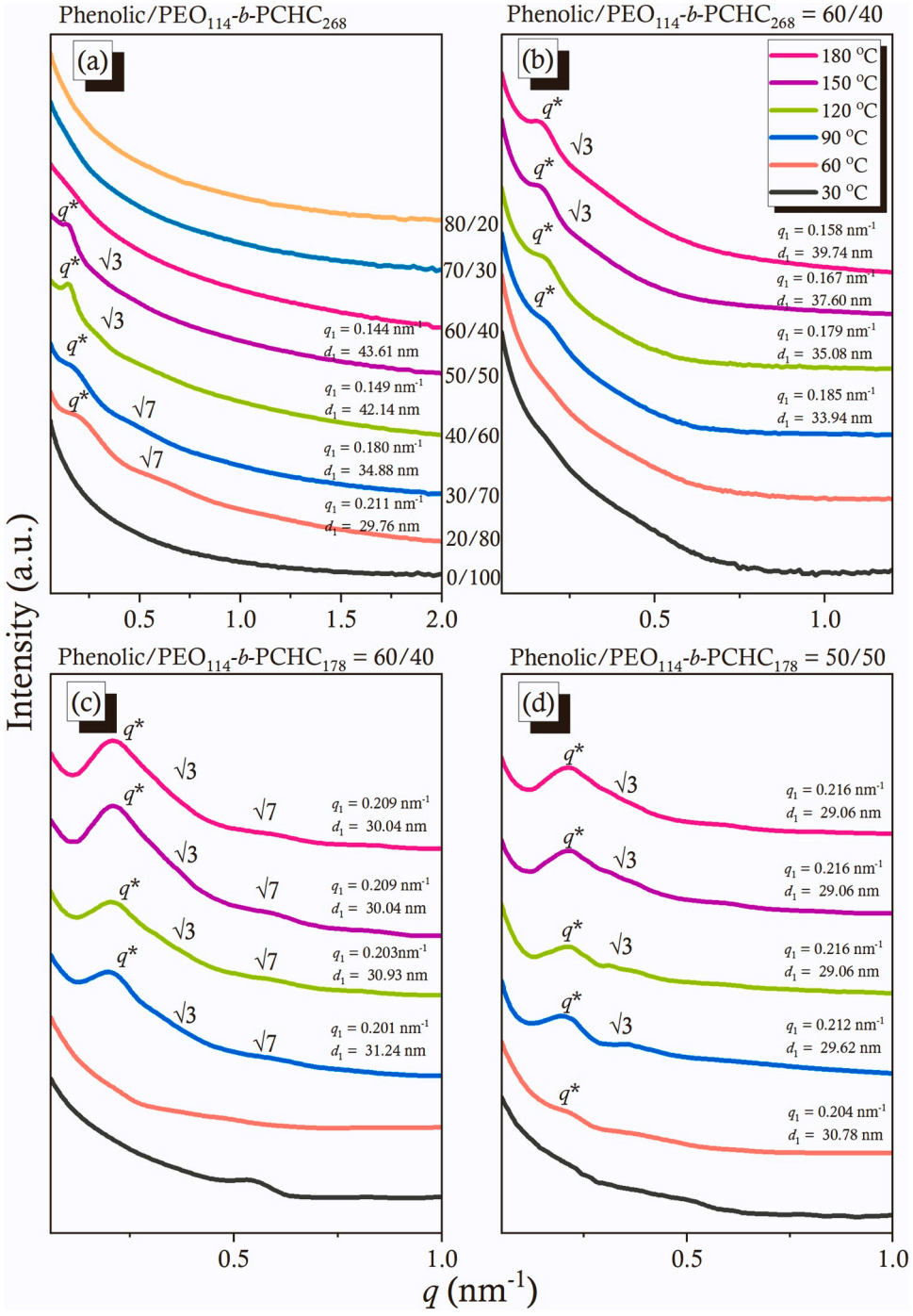

Fig. 4. (a) The SAXS of phenolic/PEO_{114}-*b*-$PCHC_{268}$ blending with various ratios at room temperature; (b) The temperature-dependent of SAXS patterns of phenolic/PEO_{114}-*b*-$PCHC_{268}$ = 60/40 blend, (c) phenolic/PEO_{114}-*b*-$PCHC_{178}$ = 60/40 blend, (d) phenolic/PEO_{114}-*b*-$PCHC_{178}$ = 50/50 blend.

again due to the OH units of phenolic both interacted with PEO ether units and PCHC C═O units based on DSC (single T_g value) and FTIR analyses.

More interesting, phenolic/PEO_{114}-*b*-$PCHC_{268}$ = 60/40 blend exhibited a very broad peak as displayed in Fig. 4(b); however, those peaks became more pronounced as thermal curing temperature increasing with peaks ratios of 1:$\sqrt{3}$ at 180 °C, also suggesting the cylindrical structure. Clearly, this self-assembled cylindrical structure was transformed much ordered with the increase of thermal curing temperature. For instance, the $\sqrt{3}$ scattering peak was only observed and the first q^* peak became sharper at temperature higher than 150 °C because of the reaction-induced microphase separation mechanism. The entropy of mixing was typically decreased during thermal polymerization because the molecular weight of phenolic resin substantially increased. This reduction in entropy is unfavorable and results in the unfavorable Gibbs free energy, leading to the formation of microphase separation and self-assembled structures. In addition, the first q^* peak was moved to relative lower q value with the increase of thermal polymerization temperature because of thermal expansion as expected at this blend system. For example, the $q^* = 0.185\ nm^{-1}$, $d = 33.94$ nm at 90 °C and $q^* = 0.158\ nm^{-1}$, $d = 39.74$ nm at 180 °C for phenolic/PEO_{114}-*b*-$PCHC_{268}$ = 60/40 blend. The similar situation was observed for phenolic/PEO_{114}-*b*-$PCHC_{178}$ = 60/40 and 50/50 blends as displayed in Fig. 4(c) and (d), the obvious peak ratios of 1:$\sqrt{3}$:$\sqrt{7}$ were observed upon increasing thermal curing temperature.

3.3. Mesoporous phenolic/carbon templated by PEO-b-PCHC diblock copolymers

To prepare the mesoporous phenolic resin templated by PEO-*b*-PCHC, the thermal properties of pure PEO-*b*-PCHC diblock copolymers were assessed through TGA analyses as shown in Fig. 2(b), the relative lower thermal decomposition behavior was observed than that of pure PEO and PCHC homopolymers, which is more suitable as the templates for desired application. Thermal calcination at 350 °C was used to remove PEO-*b*-PCHC template in this study, which is the same of PEO-*b*-PCL diblock copolymer template to obtain mesoporous phenolic resin [9]. Fig. 5 shows the selected SAXS analyses for comparison before and after thermal calcination at 350 °C from phenolic/PEO_{114}-*b*-$PCHC_{268}$ = 40/60 and 50/50 blends. Clearly, the first q^* peaks became sharper and were shifted to a higher q^* value after thermal pyrolysis, indicating the formation and the shrinkage of mesoporous structure as expected [9, 20].

For example, the $q^* = 0.140\ nm^{-1}$, $d = 44.85$ nm at 150 °C and $q^* = 0.152\ nm^{-1}$, $d = 41.31$ nm at 350 °C from phenolic/PEO_{114}-*b*-$PCHC_{268}$ = 40/60 blend and the $q^* = 0.137\ nm^{-1}$, $d = 45.83$ nm at 150 °C and $q^* = 0.147\ nm^{-1}$, $d = 42.72$ nm at 350 °C from phenolic/PEO_{114}-*b*-$PCHC_{268}$ = 50/50 blend. This observation demonstrates the transformation of the mesoporous structure upon thermal pyrolysis in this study.

Fig. 6 shows SAXS patterns and TEM images of all mesoporous phenolic resins templated by PEO_{114}-*b*-$PCHC_{268}$ diblock copolymer measured at room temperature. Fig. 6(a) displays the worm-like structure with the peak ratio of 1:$\sqrt{7}$ based on SAXS pattern and could be confirmed by TEM image in Fig. 6(d) for mesoporous phenolic resin from phenolic/PEO_{114}-*b*-$PCHC_{268}$ = 30/70 blend. Increasing phenolic compositions, Fig. 6(b), (c) and 6(g) shows the SAXS patterns of mesoporous phenolic resins formed from phenolic/PEO_{114}-*b*-$PCHC_{268}$ = 40/60, 50/50 and 60/40 blends, indicating much more ordered cylindrical structures with the peak ratios of 1:$\sqrt{3}$, as also confirmed by TEM images in Fig. 6(e), (f) and (j), respectively. Further increasing phenolic compositions, the disorder structures were observed from the phenolic/PEO_{114}-*b*-$PCHC_{268}$ = 70/30 and 80/20 blends based on SAXS patterns (Fig. 6(h) and (i)) and TEM images (Fig. 6(k) and (l)). As a result, we could conclude that at relative lower phenolic compositions (< 30 wt%), this blend system lacks sufficient phenolic resin relative to the PEO-*b*-PCHC diblock copolymer and the fraction of hydrogen bonded C═O unit of PCHC segment was relative lower compared with at higher phenolic compositions as shown in Fig. 3(d) and thus disorder or short-range order structured was observed. At relative higher phenolic

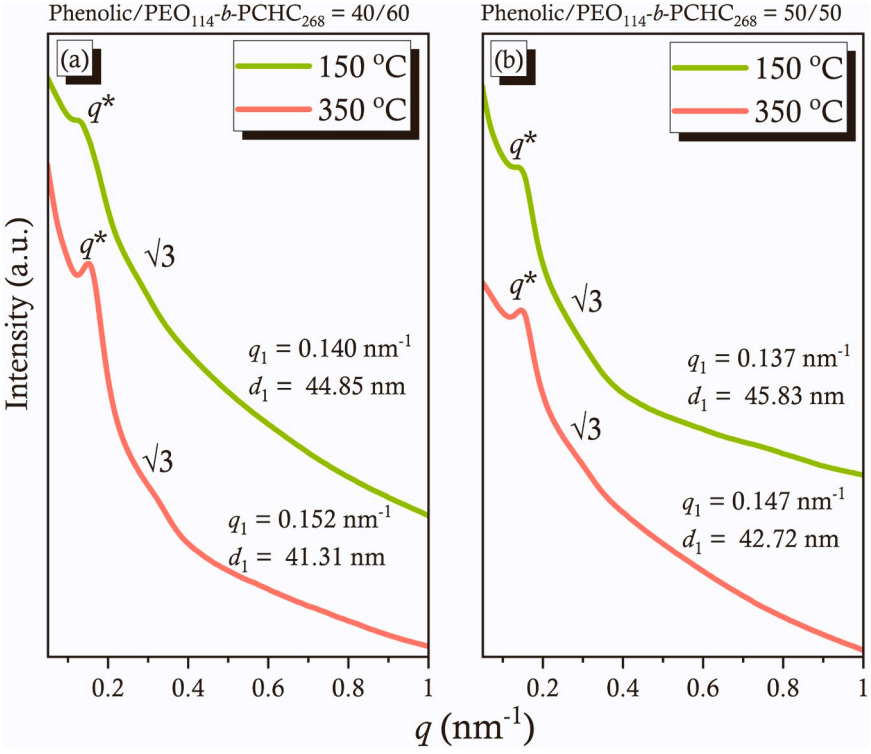

Fig. 5. The SAXS comparison of thermal curing at 150 °C and thermal calcination at 350 °C from (a) phenolic/PEO_{114}-*b*-$PCHC_{268}$ = 40/60 and (b) phenolic/PEO_{114}-*b*-$PCHC_{268}$ = 50/50 blends.

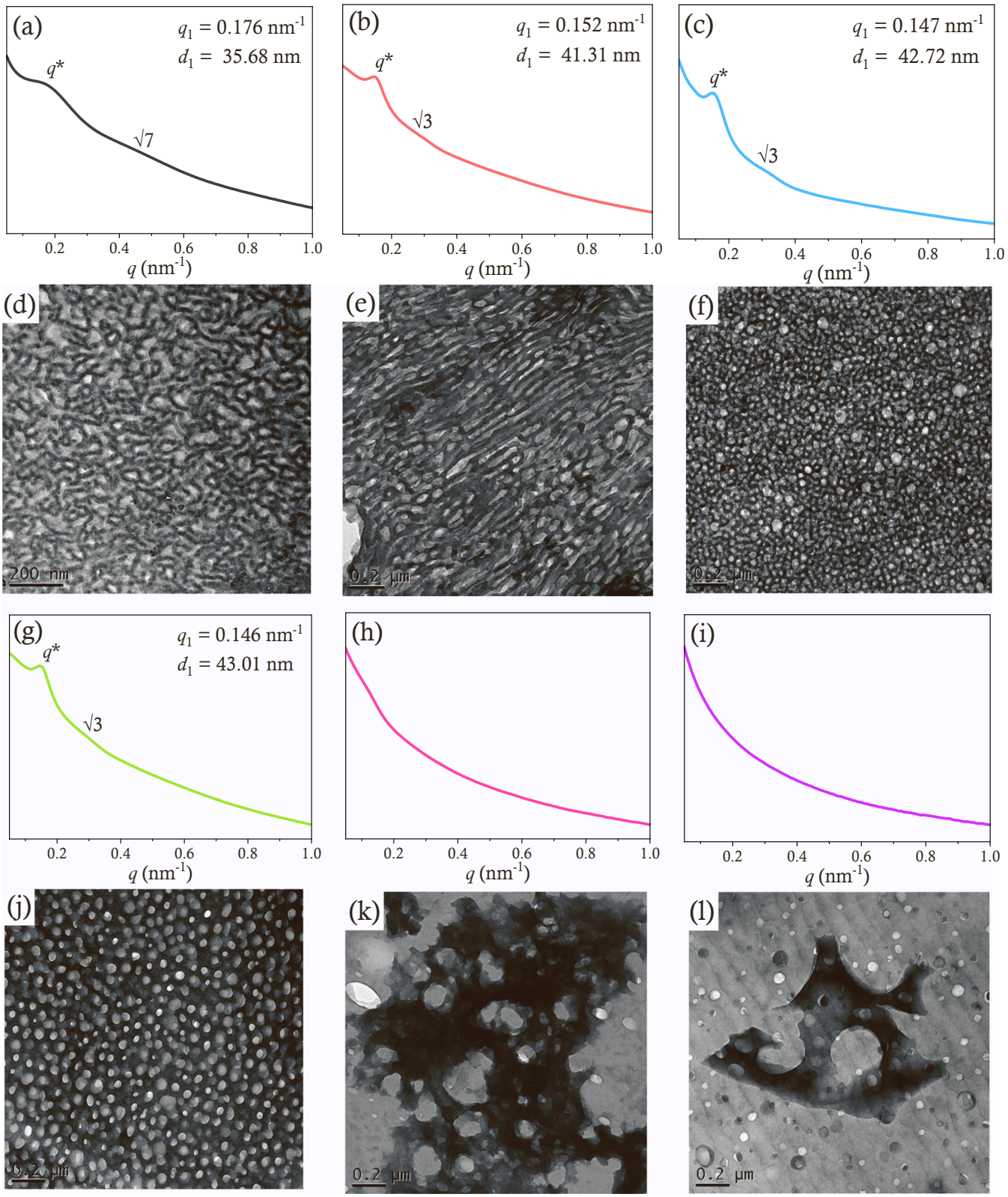

Fig. 6. The SAXS patterns and TEM images of mesoporous phenolic resins formed from phenolic/PEO_{114}-*b*-$PCHC_{268}$ = (a, d) 30/70, (b, e) 40/60, (c, f) 50/50, (g, j) 60/40, (h, k) 70/30, and (i, l) 80/20, respectively.

compositions (> 70 wt%), the OH units of phenolic resin were both interacted with PEO and PCHC segment and thus the disorder structure was formed. We could expect that the ordered mesoporous structure was only observed at phenolic compositions (40–60 wt%) through mediated by competitive hydrogen bonding interactions, which was similarly with both H-bonded acceptor diblock copolymer segments such as PEO-*b*-PCL, PEO-*b*-PLA, PCL-*b*-P4VP, and PEO-*b*-P4VP.

As a result, Fig. 7 only displays the SAXS patterns and TEM images of the mesoporous phenolic resin formed from phenolic/PEO_{114}-*b*-$PCHC_{178}$ = 40/60, 50/50 and 60/40 blends. All cylindrical structures

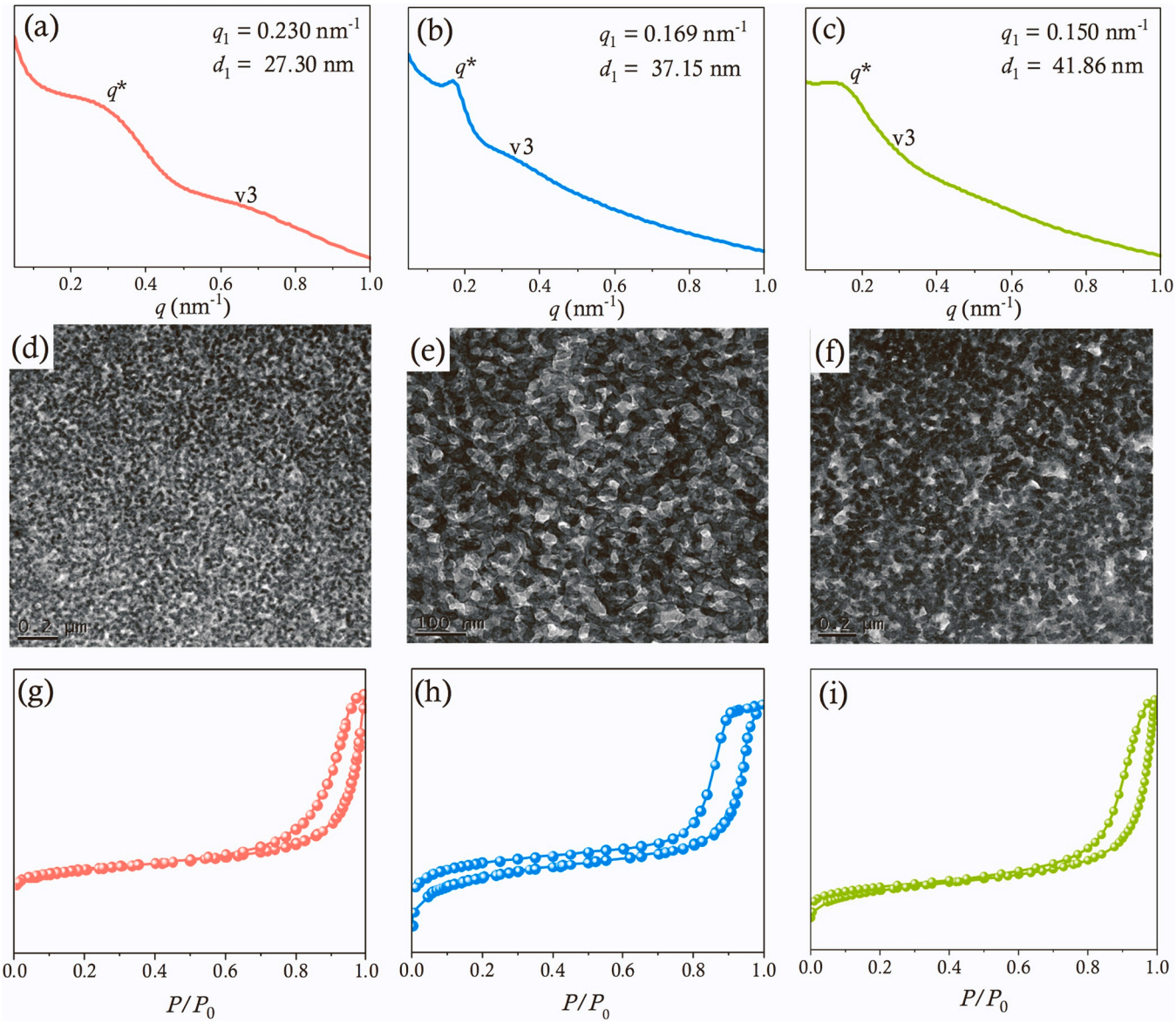

Fig. 7. The SAXS patterns, TEM images and N_2 adsorption/desorption isotherms of mesoporous phenolic resins formed from phenolic/PEO_{114}-*b*-$PCHC_{178}$ = (a, d, g) 40/60, (b, e, h) 50/50, and (c, f, i) 60/40 blends after thermal calcination at 350 °C.

were observed based on SAXS patterns with peak ratios of 1:$\sqrt{3}$ as shown in Fig. 7(a)-(c), as also confirmed by TEM images in Fig. 7(d)-(f). Their corresponding N_2 adsorption/desorption isotherms recorded at 77 K were shown in Fig. 7(g)-(i). The typical type IV curves with a sharp capillary condensation step at P/P_0 values from 0.75 to 0.98 based on the IUPAC definition and a H_1-like or H_3-like hysteresis because of cylindrical or slit-shaped mesoporous structure having a broad pore size distribution. However, the specific surface area of these mesoporous phenolic resins is ca. 60–100 m^2 g^{-1} after thermal pyrolysis and thus, the carbonization at 700 °C is considered as an efficient approach to increase the specific surface area in this study [13,27].

Fig. 8 shows SAXS, TEM and N_2 adsorption/desorption isotherms analyses of mesoporous carbons pyrolyzed from mesoporous phenolic resin derived from phenolic/PEO_{114}-*b*-$PCHC_{178}$ = 40/60, 50/50 and 60/40 blends. These patterns are the similar as those of mesoporous phenolic resin based on SAXS patterns with peak ratios of 1:$\sqrt{3}$ as shown in Fig. 8(a)-(c), as also confirmed by TEM images in Fig. 8(d)-(f). Furthermore, the d-spacing of mesoporous carbon was decreased with each blend from 27.30 nm to 25.84 nm for phenolic/PEO_{114}-*b*-$PCHC_{178}$ = 40/60 blend, from 37.15 nm to 30.33 nm for phenolic/PEO_{114}-*b*-$PCHC_{178}$ = 50/50 blend, and from 41.86 nm to 36.94 nm for phenolic/PEO_{114}-*b*-$PCHC_{178}$ = 60/40 blend, due to the complete removal of hydrogen, carbon and oxygen during pyrolysis at 700 °C. Therefore, we subsequently employ Raman spectroscopy to confirm that there has not been a substantial collapse in the mesoporous carbons. The two signals exhibited in Fig. S4 that D band at 1326 cm^{-1} for disorder carbon and G band at 1590 cm^{-1} for sp^2-bonded carbon. The ratio of I_D/I_G could be determined the graphitization degree which the range of 0.97–0.99 suggests graphite crystallites, but the ratio more than 2 indicates highly disordered carbon [27,55,56]. However, the ratio of I_D/I_G of these three mesoporous carbons are approximately 1.0 which close to graphite crystallites, suggesting that the structures did not break down by thermal treatment at 700 °C. In addition, the specific surface area of the three mesoporous carbons were measured by N_2 adsorption/desorption profiles revealed in Figs. 8(g)-8(i). Firstly, the specific surface area was significantly increased to 509, 488 and 446 m^2 g^{-1} of mesoporous carbons with average porous size around 16.2, 17.1, and 24.7 nm formed from phenolic/PEO_{114}-*b*-$PCHC_{178}$ = 40/60, 50/50 and 60/40 blends, respectively (Fig. S5). Secondly, all the mesoporous carbons are maintained the type IV curves; but a H_3-like hysteresis was found from

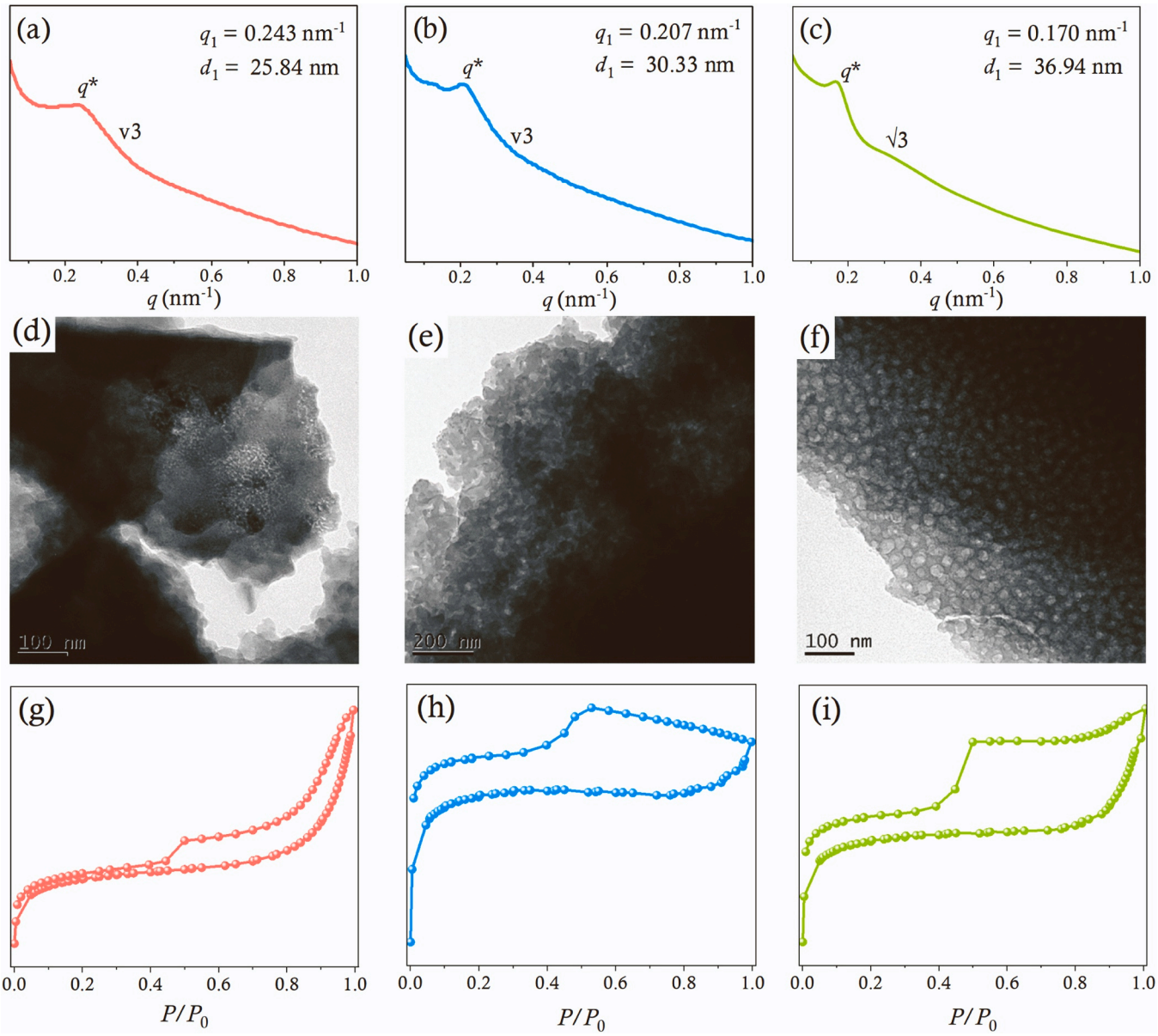

Fig. 8. The SAXS patterns, TEM images and N_2 adsorption/desorption isotherms of mesoporous carbons formed from phenolic/PEO_{114}-*b*-$PCHC_{178}$ = (a, d, g) 40/60, (b, e, h) 50/50, and (c, f, i) 60/40 blends after thermal calcination at 700 °C.

phenolic/PEO_{114}-*b*-$PCHC_{178}$ = 40/60 blend, indicating a slit-shaped mesoporous structure. Finally, the H_2-like hysteresis was observed from phenolic/PEO_{114}-*b*-$PCHC_{178}$ = 50/50 and 60/40 blend, indicating the presence of cage-like and large buckled cylindrical structures.

Since these mesoporous carbons possess high surface area, pore volume and excellent thermal stability that could effectively capture CO_2 gas as shown in Fig. 9 at 298 K and 273 K, respectively. The amount of CO_2 adsorption at 273 K are much higher than those at 298 K due to slower movement of CO_2 at lower temperature and the sequence for the amount of CO_2 capture follows the order: 40/60 (4.5 mmol g^{-1} at 273 K and 3.2 mmol g^{-1} at 298 K) > 50/50 (4.1 mmol g^{-1} at 273 K and 3.0 mmol g^{-1} at 298 K) > 60/40 (4.0 mmol g^{-1} at 273 K and 2.8 mmol g^{-1} at 298 K) blends, which is consistent with their specific surface areas. These CO_2 capture capacities of our mesoporous carbons has a much higher value (4.50 mmol g^{-1}) compared with other previously porous materials [57–60]. This is a great interesting application of these mesoporous carbons for CO_2 capture, especially considering that they were derived from the CO_2-based diblock copolymers as templates. In addition, these captured CO_2 by these materials could be recycled and employed in ROCOP again for synthesizing CO_2-based diblock copolymers, aligning perfectly with the principles of a circular economy.

4. Conclusions

We synthesized two CO_2-based PEO-*b*-PCHC diblock copolymers with a constant molecular weight of PEO but varying molecular weights of PCHC. Their chemical structures and thermal properties were confirmed by using DSC, TGA, FTIR, ^{1}H and ^{13}C NMR spectroscopy. The single T_g values demonstrated the miscible behavior of PEO-*b*-PCHC because these two block segments interacted each other through weak hydrogen bonding or dipole-dipole interaction. However, after blending with phenolic resin, the initially miscible behavior of PEO-*b*-PCHC diblock copolymer was transformed to the immiscible behavior due to the different completive hydrogen bonding strength that the OH units of phenolic was preferred to interact with the ether units of PEO rather than the C═O units of PCHC and thus the PCHC segment would form the microphase separation and self-assembled worm-like or cylindrical structure from the miscible phenolic/PEO domains at relative lower

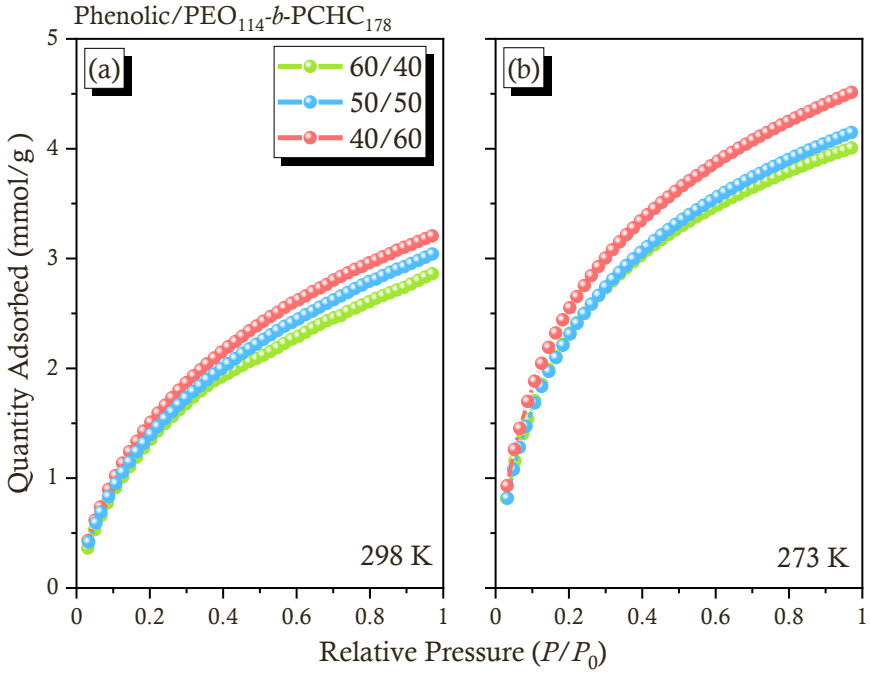

Fig. 9. CO_2 adsorption curve of mesoporous carbons formed from various phenolic/PEO_{114}-*b*-$PCHC_{178}$ blends recorded at (a) 298 K and (b) 273 K.

phenolic compositions (< 60 wt%). However, further increasing phenolic compositions, the single T_g values were observed at higher phenolic composition (> 60 wt%) due to the OH units of phenolic both interacted with the ether units of PEO and the C═O units of PCHC. Furthermore, the self-assembled cylindrical structure was transformed more ordered upon increasing thermal curing temperature at 180 °C because of the reaction-induced microphase separation mechanism. We further prepared mesoporous phenolic resin or carbon through the removal of PEO-*b*-PCHC template at 350 °C or carbonization at 700 °C, the mesoporous structures were maintained compared with phenolic/PEO-*b*-PCHC blends that the ordered mesoporous structure was only observed at phenolic compositions (40–60 wt%) through mediated by competitive hydrogen bonding interactions. These mesoporous carbons exhibited impressive characteristics such as high surface areas (> 500 m^2 g^{-1}) and they demonstrated effective CO_2 capture capabilities (4.5 mmol g^{-1} at 273 K). The captured CO_2 could subsequently be employed in ROCOP again for synthesizing CO_2-based copolymers, aligning with the principles of a circular economy.

CRediT authorship contribution statement

Du Wei-Ting: Writing – original draft, Formal analysis, Data curation, Conceptualization. **Chen Shih-Yun:** Investigation, Formal analysis, Data curation. **Kuo Shiao Wei:** Writing – review & editing, Supervision, Resources, Funding acquisition, Conceptualization.

Declaration of Competing Interest

The authors declare that they have no known competing financial interests or personal relationships that could have appeared to influence the work reported in this paper.

Data Availability

The data that has been used is confidential.

Acknowledgments

This study was supported financially by the Ministry of Science and Technology, Taiwan, under contracts NSTC 112-2218-E-110-007, and 112-2223-E-110-004. The authors thank the staff at National Sun Yat-sen University for their assistance with the TEM (ID: EM022600) experiments.

Authors of the manuscript

Declaration of interest.

Supporting information available

FTIR and Raman spectra of PEO-*b*-PCHC diblock copolymer and their corresponding characterization analyses.

Appendix A. Supporting information

Supplementary data associated with this article can be found in the online version at doi:10.1016/j.jcou.2024.102702.

References

[1] I.M. Lin, R.H. Tsai, Y.T. Chou, Y.W. Chiang, Photonic crystal reflectors with ultrahigh sensitivity and discriminability for detecting extremely low-concentration surfactants, ACS Appl., Mater. Interfaces 15 (2023) 45249–45259, https://doi.org/10.1021/acsami.3c06946.
[2] S.M. Liu, Y. Yang, L.B. Zhang, J.P. Xu, J.T. Zhu, Recent progress in responsive photonic crystals of block copolymers, J. Mater. Chem. C. 8 (2020) 16633–16647, https://doi.org/10.1039/D0TC04561F.
[3] A.M. Jazani, J.K. Oh, Development and disassembly of single and multiple acid-cleavable block copolymer nanoassemblies for drug delivery, Polym. Chem. 11 (2020) 2934–2954, https://doi.org/10.1039/D0PY00234H.
[4] J. Diaz, M. Pinna, C. Breen, A. Zvelindovsky, I. Pagonabarraga, Block copolymer nanocomposites under confinement: effect on frustrated phases, Macromolecules 56 (2023) 5010–5021, https://doi.org/10.1021/acs.macromol.3c00166.
[5] K.C. Yang, P. Puneet, P.T. Chiu, R.M. Ho, Well-ordered nanonetwork metamaterials from block copolymer templated syntheses, Acc. Chem. Res. 55 (2022) 2033–2042, https://doi.org/10.1021/acs.accounts.2c00152.
[6] W. Wang, C. Wu, R. Sun, D. Li, H. Ru, Simple and controllable preparation of SBA-15 microspheres by poly(vinyl alcohol)-assisted P123 templating system,

Microporous Mesoporous Mater. 302 (2020) 110211, https://doi.org/10.1016/j.micromeso.2020.110211.
[7] W.-C. Chu, S.-F. Chiang, J.-G. Li, S.-W. Kuo, Hydrogen bonding-mediated microphase separation during the formation of mesoporous novolac-type phenolic resin templated by the triblock copolymer, PEO-b-PPO-b-PEO, Materials 6 (2013) 5077–5093, https://doi.org/10.3390/ma6115077.
[8] W.C. Chu, S.F. Chiang, J.G. Li, S.W. Kuo, Mesoporous silicas templated by symmetrical multiblock copolymers through evaporation-induced self-assembly, RSC Adv. 4 (2014) 784–793, https://doi.org/10.1039/C3RA45348K.
[9] S.W. Kuo, Hydrogen bonding mediated self-assembled structures from block copolymer mixtures to mesoporous materials, Polym. Int. 71 (2022) 393–410, https://doi.org/10.1002/pi.6264.
[10] A.F.M. EL-Mahdy, T.C. Yu, S.-W. Kuo, Synthesis of multiple heteroatom–doped mesoporous carbon/silica composites for supercapacitors, Chem. Eng. J. 414 (2021) 128796, https://doi.org/10.1016/j.cej.2021.128796.
[11] J.-G. Li, Y.-D. Lin, S.-W. Kuo, From microphase separation to self-organized mesoporous phenolic resin through competitive hydrogen bonding with double-crystalline diblock copolymers of poly(ethylene oxide-b-ε-caprolactone), Macromolecules 44 (2011) 9295–9309, https://doi.org/10.1021/ma2010734.
[12] A.F.M. El-Mahdy, T.-E. Liu, S.-W. Kuo, Direct synthesis of nitrogen-doped mesoporous carbons from triazine-functionalized resol for CO_2 uptake and highly efficient removal of dyes, J. Hazard. Mater. 391 (2020) 122163, https://doi.org/10.1016/j.jhazmat.2020.122163.
[13] J.G. Li, Y.F. Ho, M.M.M. Ahmed, H.C. Liang, S.W. Kuo, Mesoporous carbons templated by PEO-PCL block copolymers as electrode materials for supercapacitors, Chem. – Eur. J. 25 (2019) 10456–10463, https://doi.org/10.1002/chem.201901724.
[14] C.-C. Tsai, Z. Gan, S.-W. Kuo, Using benzoxazine chemistry and bio-based triblock copolymer to prepare functional porous polypeptide capable of efficient dye adsorption, Polym. Chem. 9 (2018) 3684–3693, https://doi.org/10.1039/c8py00664d.
[15] Y. Kang, O. Cretu, J. Kikkawa, K. Kimoto, H. Nara, A.S. Nugraha, H. Kawamoto, M. Eguchi, T. Liao, Z. Sun, T. Asahi, Y. Yamauchi, Mesoporous multimetallic nanospheres with exposed highly entropic alloy sites, Nat. Commun. 14 (2023) 4182, https://doi.org/10.1038/s41467-023-39157-2.
[16] J.G. Li, P.Y. Lee, M.M.M. Ahmed, M.G. Mohamed, S.W. Kuo, Varying the hydrogen bonding strength in Phenolic/PEO-b-PLA blends provides mesoporous carbons having large accessible pores suitable for energy storage, Macromol. Chem. Phys. 221 (2020) 2000040, https://doi.org/10.1002/macp.202000040.
[17] M.G. Mohamed, W.-S. Hung, A.F.M. EL-Mahdy, M.M.M. Ahmed, L. Dai, T. Chen, S.-W. Kuo, High-molecular-weight PLA-b-PEO-b-PLA triblock copolymer templated large mesoporous carbons for supercapacitors and CO_2 capture, Polymers 12 (2020) 1193, https://doi.org/10.3390/polym12051193.
[18] E. Bloch, P.L. Llewellyn, T. Phan, D. Bertin, V. Hornebecq, On defining a simple empirical relationship to predict the pore size of mesoporous silicas prepared from PEO-b-PS diblock copolymers, Chem. Mater. 21 (2009) 48–55, https://doi.org/10.1021/cm801978w.
[19] V. Perazzolo, G. Daniel, R. Brandiele, Picelli, L.G.A. Rizzi, A.A. Isse, C. Durante, PEO-b-PS block copolymer templated mesoporous carbons: a comparative study of nitrogen and sulfur doping in the oxygen reduction reaction to hydrogen peroxide, Chem. Eur. J. 27 (2021) 1002–1014, https://doi.org/10.1002/chem.202003355.
[20] J. Wei, Z. Sun, W. Luo, Y. Li, A.A. Elzatahry, A.M. Al-Enizi, Y. Deng, D. Zhao, New Insight into the synthesis of large-pore ordered mesoporous materials, J. Am. Chem. Soc. 139 (2017) 1706–1713, https://doi.org/10.1021/jacs.6b11411.
[21] S.W. Kuo, Construction Archimedean tiling patterns based on soft materials from block copolymers and covalent organic frameworks, Giant 15 (2023) 100170, https://doi.org/10.1016/j.giant.2023.100170.
[22] A.F.M. EL-Mahdy, T.C. Yu, M.G. Mohamed, S.W. Kuo, Secondary structures of polypeptide-based diblock copolymers influence the microphase separation of templates for the fabrication of microporous carbons, Macromolecules 54 (2021) 1030–1042, https://doi.org/10.1021/acs.macromol.0c01748.
[23] M.G. Mohamed, S.W. Kuo, Progress in the self-assembly of organic/inorganic polyhedral oligomeric silsesquioxane (POSS) hybrids, Soft Matter 18 (2022) 5535–5561, https://doi.org/10.1039/D2SM00635A.
[24] W.C. Chen, Y.T. Liu, S.W. Kuo, Mesoporous organic/inorganic hybrid materials with frank-kasper phases templated by an unusual linear symmetry diblock copolymer, Macromol. Rapid Commun. 42 (2021) e2100302, https://doi.org/10.1002/marc.202100302.
[25] W.-S. Hung, M.M.M. Ahmed, M.G. Mohamed, S.W. Kuo, Competing hydrogen bonding produces mesoporous/macroporous carbons templated by a high-molecular-weight poly (caprolactone–b–ethylene oxide–b–caprolactone) triblock copolymer, J. Polym. Res. 27 (2020) 173, https://doi.org/10.1007/s10965-020-02154-w.
[26] C.-C. Liu, W.-C. Chu, J.-G. Li, S.-W. Kuo, Mediated competitive hydrogen bonding form mesoporous phenolic resins templated by poly(ethylene oxide-b-ε-caprolactone-b-l-lactide) Triblock Copolymers, Macromolecules 47 (2014) 6389–6400, https://doi.org/10.1021/ma501246j.
[27] W.-C. Chu, B.P. Bastakoti, Y.V. Kaneti, J.-G. Li, H.R. Alamri, Z.A. Alothman, Y. Yamauchi, S.-W. Kuo, Tailored design of bicontinuous gyroid mesoporous carbon and nitrogen-doped carbon from poly(ethylene oxide-b-caprolactone) diblock copolymers, Chem. Eur. J. 23 (2017) 13734–13741, https://doi.org/10.1002/chem.201702360.
[28] Y.-C. Huang, W.-C. Chen, S.-W. Kuo, Mesoporous phenolic/poss hybrids induced by microphase separation arising from competitive hydrogen bonding interactions, Macromolecules 55 (2022) 8918–8930, https://doi.org/10.1021/acs.macromol.2c01585.
[29] T.M. McGuire, A. Buchard, C. Williams, Chemical recycling of commercial poly(L-lactic acid) to L-Lactide using a high-performance Sn(II)/alcohol catalyst system, J. Am. Chem. Soc. 145 (2023) 19840–19848, https://doi.org/10.1021/jacs.3c05863.
[30] H.-W. Ou, K.-H. Lo, W.-T. Du, W.-Y. Lu, W.-J. Chuang, B.-H. Huang, H.-Y. Chen, C.-C. Lin, Synthesis of sodium complexes supported with NNO-tridentate schiff base ligands and their applications in the ring-opening polymerization of L-Lactide, Inorg. Chem. 55 (2016) 1423–1432, https://doi.org/10.1021/acs.inorgchem.5b02043.
[31] D.J. Darensbourg, W. Choi, O. Karroonnirun, N. Bhuvanesh, Ring-opening polymerization of cyclic monomers by complexes derived from biocompatible metals. production of Poly(lactide), Poly(trimethylene carbonate), and their copolymers, Macromolecules 41 (2008) 3493–3502, https://doi.org/10.1021/ma800078t.
[32] T.M. Ovitt, G.W. Coates, Stereochemistry of lactide polymerization with chiral catalysts: new opportunities for stereocontrol using polymer exchange mechanisms, J. Am. Chem. Soc. 124 (2002) 1316–1326, https://doi.org/10.1021/ja012052.
[33] S. Paul, Y. Zhu, C. Romain, R. Brooks, P.K. Saini, C.K. Williams, Ring-opening copolymerization (ROCOP): synthesis and properties of polyesters and polycarbonates, Chem. Commun. 51 (2015) 6459–6479, https://doi.org/10.1039/C4CC10113H.
[34] C.K. Williams, Synthesis of functionalized biodegradable polyesters, Chem. Soc. Rev. 36 (2007) 1573–1580, https://doi.org/10.1039/B614342N.
[35] D. Mecerreyes, J. Robert, D. Philippe, Novel macromolecular architectures based on aliphatic polyesters relevance of the "coordination-insertion" ring-opening polymerization, Macromol. Archit. (1999) 1–59, https://doi.org/10.1007/3-540-49196-1_1.
[36] W. Lindeboom, A.C. Deacy, A. Phanopoulos, A. Buchard, C.K. Williams, Correlating metal redox potentials to Co(III)K(I) catalyst performances in carbon dioxide and propene oxide ring opening copolymerization, Angew. Chem. Int. Ed. 62 (2023) e202308378, https://doi.org/10.1002/anie.202308378.
[37] T.M. McGuire, A.C. Deacy, A. Buchard, C.K. Williams, Solid-state chemical recycling of polycarbonates to epoxides and carbon dioxide using a heterodinuclear Mg(II)Co(II) catalyst, J. Am. Chem. Soc. 144 (2022) 18444–18449, https://doi.org/10.1021/jacs.2c06937.
[38] M.-J. Li, Y.-C. Su, G.-L. Liu, B.-T. Ko, Dinuclear nickel complexes using hexadentate benzothiazole-based diamine-bisphenolate ligands: highly active catalysts for copolymerization of carbon dioxide with epoxides, Inorg. Chem. 61 (2022) 12835–12846, https://doi.org/10.1021/acs.inorgchem.2c01972.
[39] R.C. Jeske, J.M. Rowley, G.W. Coates, Pre-rate-determining selectivity in the terpolymerization of epoxides, cyclic anhydrides, and CO_2: a one-step route to diblock copolymers, Angew. Chem. Int. Ed. 47 (2008) 6041–6044, https://doi.org/10.1002/ange.200801415.
[40] M.M.S. Buchaca, F. Cruz-Martinez, L.F.S. Barba, J. Tejeda, A.M. Rodriguez, J.A. C. Osma, A.L. Sanchez, One-pot terpolymerization of CHO, CO_2 and L-lactide using chloride indium catalysts, Dalton Trans. 52 (2023) 3482–3492, https://doi.org/10.1039/D3DT00391D.
[41] C.W. Vos, J. Beament, C.M. Kozak, Ring opening polymerization and copolymerization for polyester and polycarbonate formation by a diamino-bis (phenolate) chromium(III) catalyst, Polym. Chem. 14 (2023) 5083–5093, https://doi.org/10.1039/D3PY01114C.
[42] D.J. Darensbourg, G.-P. Wu, A one-pot synthesis of a triblock copolymer from propylene oxide/carbon dioxide and lactide: intermediacy of polyol initiators, Angew. Chem. Int. Ed. 125 (2013) 10796–10800, https://doi.org/10.1002/ange.201304778.
[43] S. Paul, C. Romain, J. Shaw, C.K. Williams, Sequence selective polymerization catalysis: a new route to ABA block Copoly(ester-b-carbonate-b-ester), Macromolecules 48 (2015) 6047–6056, https://doi.org/10.1021/acs.macromol.5b01293.
[44] Y.-Y. Zhang, G.-W. Yang, Y. Wang, X.-Y. Lu, G.-P. Wu, Z.-S. Zhang, K. Wang, R.-Y. Zhang, P.F. Nealey, D.J. Darensbourg, Z.-K. Xu, Synthesis of CO_2-based block copolymers via chain transfer polymerization using macroinitiators: activity, blocking efficiency, and nanostructure, Macromolecules 51 (2018) 791–800, https://doi.org/10.1021/acs.macromol.7b02231.
[45] S.C. Tsai, Y.C. Lin, E.L. Lin, Y.W. Chiang, S.W. Kuo, Hydrogen bonding strength effect on self-assembly supramolecular structures of diblock copolymer/homopolymer blends, Polym. Chem. 7 (2016) 2395–2409, https://doi.org/10.1039/C6PY00195E.
[46] W.C. Chen, S.W. Kuo, C.H. Lu, U.S. Jeng, F.C. Chang, Self-assembly structures through competitive interactions of crystalline-amorphous diblock copolymer/homopolymer blends: Poly(ε-caprolactone-b-4-vinylpyridine)/ poly(vinyl phenol), Macromolecules 42 (2009) 3580–3590, https://doi.org/10.1021/ma900080v.
[47] W.C. Chen, S.W. Kuo, U.S. Jeng, F.C. Chang, Self-assembly through competitive interactions of miscible diblock copolymer/homopolymer blends: Poly (vinylphenol-b-methyl methacrylate)/poly (vinylpyrrolidone) blend, Macromolecules 41 (2008) 1401–1410, https://doi.org/10.1021/ma7021925.
[48] S.W. Kuo, Hydrogen bond-mediated self-assembly and supramolecular structures of diblock copolymer mixtures, Polym. Int. 58 (2009) 455–464, https://doi.org/10.1002/pi.2513.
[49] T.C. Tseng, S.W. Kuo, Hydrogen-bonding strength influences hierarchical self-assembled structures in unusual miscible/immiscible diblock copolymer blends, Macromolecules 51 (2018) 6451–6459, https://doi.org/10.1021/acs.macromol.8b00751.
[50] S.W. Kuo, Hydrogen Bonding in Polymeric Materials, John Wiley & Sons,, Hoboken, NJ, 2018, https://doi.org/10.1002/9783527804276.

[51] W.-T. Du, Y.-L. Kuan, S.-W. Kuo, Intra- and intermolecular hydrogen bonding in miscible blends of co2/epoxy cyclohexene copolymer with Poly(Vinyl Phenol), Int. J. Mol. Sci. 23 (2022) 7018, https://doi.org/10.3390/ijms23137018.
[52] S.-W. Kuo, W.-J. Huang, C.-F. Huang, S.-C. Chan, F.-C. Chang, Miscibility, specific interactions, and spherulite growth rates of binary Poly (acetoxystyrene)/Poly (ethylene oxide) Blends, Macromolecules 37 (2004) 4164–4173, https://doi.org/10.1021/ma035417e.
[53] S.-W. Kuo, C.-L. Lin, F.-C. Chang, Phase behavior and hydrogen bonding in ternary polymer blends of phenolic resin/poly (ethylene oxide)/poly (ε-caprolactone), Macromolecules 35 (2002) 278–285, https://doi.org/10.1021/ma011255f.
[54] S.W. Kuo, C.L. Lin, F.C. Chang, The study of hydrogen bonding and miscibility in Poly(vinylpyridines) with Phenolic Resin, Polymer 43 (2002) 3943, https://doi.org/10.1016/S0032-3861(02)00214-8.
[55] T.V. Reshetenko, L.B. Avdeeva, Z.R. Ismagilov, V.V. Pushkarev, S.V. Cherepanova, A.L. Chuvilin, V.A. Likholobov, Catalytic filamentous carbon: structural and textural properties, Carbon 41 (2003) 1605–1615, https://doi.org/10.1016/S0008-6223(03)00115-5.
[56] A. Vinu, P. Srinivasu, M. Takahashi, T. Mori, V.V. Balasubramanian, K. Ariga, Controlling the textural parameters of mesoporous carbon materials, Microporous Mesoporous Mater. 100 (2007) 20–26, https://doi.org/10.1016/j.micromeso.2006.10.008.
[57] A.O. Mousa, C.-H. Chuang, S.-W. Kuo, M.G. Mohamed, Strategic design and synthesis of ferrocene linked porous organic frameworks toward tunable CO_2 capture and energy storage, Int. J. Mol. Sci. 24 (2023) 12371, https://doi.org/10.3390/ijms241512371.
[58] A.O. Mousa, M.G. Mohamed, C.-H. Chuang, S.-W. Kuo, Carbonized aminal-linked porous organic polymers containing pyrene and triazine units for gas uptake and energy storage, Polymers 15 (2023) 1891, https://doi.org/10.3390/polym15081891.
[59] A.F.M. EL-Mahdy, C. Young, J. Kim, J. You, Y. Yamauchi, S.W. Kuo, Hollow microspherical and microtubular [3 + 3] carbazole-based covalent organic frameworks and their gas and energy storage applications, ACS Appl. Mater. Interfaces 11 (2019) 9343–9354, https://doi.org/10.1021/acsami.8b21867.
[60] M.G. Mohamed, T.-C. Chen, S.-W. Kuo, Solid-state chemical transformations to enhance gas capture in benzoxazine-linked conjugated microporous polymers, Macromolecules 54 (2021) 5866–5877, https://doi.org/10.1021/acs.macromol.1c00736.